HOSTED BY

Available online at www.sciencedirect.com
ScienceDirect
Journal of Radiation Research and Applied Sciences
journal homepage: http://www.elsevier.com/locate/jrras

Estimation of the spatial energy deposition in CA1 pyramidal neurons under exposure to ^{12}C and ^{56}Fe ion beams

Munkhbaatar Batmunkh [a,b,*], *Oleg V. Belov* [a], *Lkhagvaa Bayarchimeg* [a], *Oidov Lhagva* [b], *Nasser H. Sweilam* [c]

[a] *Laboratory of Radiation Biology, Joint Institute for Nuclear Research, 6 Joliot-Curie St., 141980 Dubna, Moscow Region, Russia*
[b] *Natural Science Division, National University of Mongolia, 1 University St., Sukhbaatar District, 210646 Ulaanbaatar, Mongolia*
[c] *Mathematics Department, Faculty of Science, Cairo University, Giza 12613, Egypt*

ARTICLE INFO

Article history:
Received 12 January 2015
Accepted 25 May 2015
Available online 6 June 2015

Keywords:
Radiation risk
HZE particles
Monte Carlo simulation
Neurons

ABSTRACT

The exposure to heavy charged particles represents a significant risk to the central nervous system. In experiments with rodents, the irradiation with heavy ions induces a prolonged deficit in hippocampus-dependent learning and memory. The exact nature of these violations remains mostly unclear. In this regard, the estimation of radiation effects at the level of single neurons is of our special interest. The present study demonstrates the results of comparative calculations that are performed to clarify the early physical events in single neurons under the exposure to accelerated ^{12}C and ^{56}Fe ions with different parameters. Using the Geant4-based Monte Carlo simulations, the radiation effects are considered in terms of energy and dose deposition. The spatial patterns of energy and dose depositions within a single neural cell are produced. As additional characteristics, the spectra of the specific energy and energy imparted are estimated. Our results show that the cell morphology is an important factor determining the accumulation of radiation dose in neurons under the exposure to heavy ions. The data obtained suggest a possibility of radiation damage to synapses that are considered to play an important role in radiation-induced violations of hippocampus-dependent learning and memory.

* *Corresponding author*. Laboratory of Radiation Biology, Joint Institute for Nuclear Research, 6 Joliot-Curie St., 141980 Dubna, Moscow Region, Russia. Tel.: +7 4962162847.
E-mail address: batmunkhm@hotmail.com (M. Batmunkh).

Peer review under responsibility of The Egyptian Society of Radiation Sciences and Applications.
http://dx.doi.org/10.1016/j.jrras.2015.05.008

1. Introduction

Within the last few years, radiation damage to the central nervous system (CNS) has become an increasingly important field of research for two major reasons. First one is represented by the ongoing preparation of deep-space manned flights. For these missions, the prediction of the health risk from space radiation is one of the crucial tasks. The second reason is determined by the estimation of possible side effects of brain cancer therapy with hadron beams.

Recent findings suggest that the exposure to space radiation could be a significant limitation to human traveling beyond the Earth's magnetosphere. In contrast to the delayed consequences of radiation exposure (cancer, cataracts, cytogenetic disturbances, a decrease in lifespan, etc.), CNS risk may affect the performance and astronauts' health directly in flight. The effects which can arise during the mission embrace altered cognitive function, including detriments in short-term memory, reduced motor function, and behavioral changes. Late CNS violations may be represented by a variety of neurological disorders such as accelerated aging, Alzheimer's disease and other cognitive impairments (Cucinotta, Alp, Sulzman, & Wang, 2014; Machida, 2009). At the present, the mechanisms behind these malfunctions are mostly unknown.

The most harmful factors of space radiation risk are the galactic cosmic rays (GCRs) and solar particle events (SPEs). Both GCRs and SPEs are composed of high-energy protons, alpha-particles, and a relatively small amount of high-Z and energy (HZE) particles (Cucinotta, Townsend, Wilson, Golightly, & Weyland, 1994; Kim et al., 1999; NCRP, 1989; Townsend, Cucinotta, Wilson, & Bagga, 1994; Wiebel, 1994). GCR energies range from less than 10 MeV/u to above 10,000 MeV/u with median energies inside tissue of about 1500 MeV/u for HZE components and several hundred MeV for protons and helium nuclei (Cucinotta et al., 2014). SPEs are of much lower energy than GCRs and occur at more modest dose-rates. Spacecraft shielding is an effective countermeasure to SPEs, but not to HZE particles of GCRs. Although HZE nuclei constitute a modest part of the total physical radiation dose, they are a large component of the biological radiation dose, due to their high linear energy transfer (LET) and a more complicated energy deposition pattern.

On the other hand, radiotherapy of brain tumors is another potential risk of functional violations in the CNS. A number of documented evidences reviewed in (Cucinotta, Wang, & Huff, 2009; Cucinotta et al., 2014) suggest neurological complications associated with cancer therapy employing ionizing radiations. In this regard, radiotherapy with heavy ions (for example ^{12}C, as the most widespread) represents a major jeopardy due the high relative biological effectiveness (RBE) of these particles (Schardt, Elsasser, & Schulz-Ertner, 2010; Wang et al., 2005; Yasuda et al., 2011).

The particle traversals to neurons are the initial events of radiation damage to the CNS. In several papers we found estimations of total number of particle-track traversals per neural cell during space missions (Cucinotta, Nikjoo, & Goodhead, 1998; Curtis et al., 1998; Gauger, Tobias, Yang, & Whitney, 1986; Yasuda, Komiyama, & Fujitaka, 2001). Fewer data pieces, however, are available on patterns of HZE particle energy deposition inside individual neurons. Except the preliminary Monte Carlo calculations made by Alp, Limoli, and Cucinotta (Cucinotta et al., 2014), we didn't observe any attempts in this filed. Many of the previous microdosimetric simulations and measurements, investigating the radiation response over the simplification of cell model (i.e., usually spheres or cubes), have not modeled the shape, size, or complex cell structures (Latocha et al., 2007; Palajová, Spurny, & Davídková, 2006; Rollet et al., 2011). The present paper provides several examples of energy deposition simulations in neurons irradiated by ^{12}C and ^{56}Fe ions with energies, corresponding to the maximal GCR differential flux. For this purpose, the Monte Carlo-based microdosimetric technique is used together with a precise simulation of the neural cell morphology.

In our work, pyramidal neurons of the CA1 hippocampal field are selected for the analysis. The hippocampus itself represents a brain area which is frequently associated with radiation-induced impairments in cognitive functions (Bannerman et al., 2014; Britten et al., 2012; Machida, 2009; Rola et al., 2008; Rudobeck, Nelson, Sokolova, & Vlkolinský, 2014). The activity of CA1 field is thought to be essential for spatial learning and memory, i.e. for those CNS functions that are highly disturbed by irradiation with HZE particles.

2. Materials and methods

2.1. *Neuron morphology*

Typically, neuron cells are composed of a cell body (soma), axon, and a dendritic tree. A soma contains the cell nucleus and all of the other organelles that are needed to keep the cell functioning. An axon is a long fiber, sometimes branched, which arises from the soma and extends for a long distance up to 1 m in humans. Dendrites are thin appendages that also arise from the soma and get narrower as they extend further away from the cell body. Dendrites are much shorter than axons. They can extend for hundreds of micrometers branching and forming a complicate dendritic tree. The latter includes thousands of dendritic spines which are tiny compartments that protrude from the dendrites and form the post-synaptic compartment of synapses.

In order to simulate the morphology of a CA1 hippocampal neuron, the original data from NeuroMorpho.Org data-base (Ascoli, 2006; Carnevale, Tsai, Claiborne, & Brown, 1997) is employed. The pyramidal neuron of an adult Sprague-Dawley male rat (cell ID: NMO_00445; neuron name: 5038804) is selected for the analysis. The major morphological parameters of this cell are presented in Table 1. According to our calculations, individual components of the neuron are simulated by spherical and cylindrical volumes. In so doing, the soma is represented by combination of several spheres, while the dendritic tree is described with combinations of cylinders (Fig. 1). The sphere diameters within the soma area are ranged from 3.6 to 13.52 μm. The diameters and lengths of the cylinders simulating dendrites are in the ranges of 0.9–4.96 μm and 1.35–22.56 μm, respectively. In our spatial model, 9 spheres and 2224 cylinders are used. Since the neural cell selected for

Table 1 – Major morphological parameters of the pyramidal neuron ID:NMO_00445 (neuron name 5038804), as it is presented in the NeuroMorpho.Org data-base (Ascoli, 2006; Carnevale et al., 1997).

Parameter	Value
Total surface	54.77×10^3 μm^2
Total volume	20.92×10^3 μm^3
Soma surface	0.18×10^3 μm^2
Number of branches	171
Number of bifurcations	84
Overall width	219.18 μm
Overall height	681.26 μm
Overall depth	133.34 μm
Average diameter	1.48 μm

the consideration has no axon, we don't assign any representation for this component.

2.2. *Microdosimetric calculations*

For the purpose of simulating the energy deposition inside the neuron traversed by a HZE particle, the coordinates of cell components are translated from the SWC file format of NeuroMorpho.Org data-base and imported into the Geant4 simulation toolkit (version 9.5), capable to simulate HZE particle track structures (Agostinelli et al., 2003; Allison et al., 2006). A standard microdosimetric technique implemented in this toolkit is applied to the neuron model composed of various segments (i.e., spheres and cylinders). For the positioning and rotation of neuron segments, we have written the daughter-class script using a special parameterization class named *G4VPV Parameterisation* (Geant4 Virtual class for Parameterized Volumes). It allows each segment to be different not only in position and rotational angle, but in material, size, and shape as well. To avoid an overestimation of the neuron volume, a special procedure is created to check, whether any of the segments overlapped or not. For this purpose the Boolean operators are used in the parameterization class. If overlapping segments are detected, one of the intersecting areas becomes disabled.

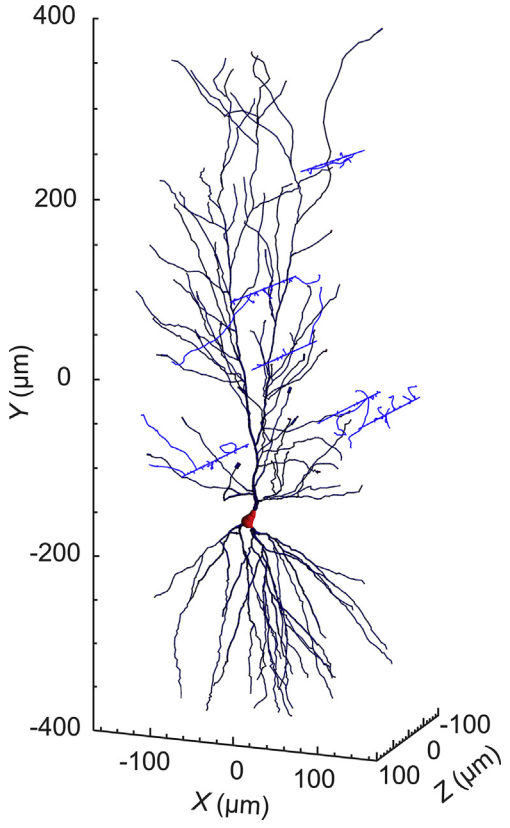

Fig. 1 – Three-dimensional projection of the rat CA1 hippocampal neuron combined with six tracks of ^{12}C ions. The topological data on neuron morphology is taken from the NeuroMorpho.Org data-base (Ascoli, 2006; Carnevale et al., 1997). The cell ID is NMO_00445; the neuron name is 5038804.

The trajectories of HZE particle tracks are simulated in 800 × 300 × 200 μm box of 48 × 10^6 μm^3 volume filled with liquid water. The liquid water is also used as the intracellular medium of the neuron placed in the same box (Fig. 1).

Our microdosimetric calculations estimate the distribution of the energy deposits $\varepsilon_i(x, y, z)$ at the spatial coordinates x, y, and z of each particle track traversing the pyramidal neuron. This distribution enables to obtain stochastic quantities such as the energy imparted and specific energy (ICRU, 2011). Both quantities are connected with the relative biological effectiveness (RBE) of HZE particles (Okamoto et al., 2011; Schmid & Schrader, 2007).

The energy imparted, ε, is the sum of all energy depositions to the mater in a given volume, defined as $\varepsilon = \sum_j \varepsilon_i(x, y, z)$. Using this quantity, the amount of radiation energy imparted to a segment of pyramidal neuron of the mass dm_i can be defined as the absorbed dose, *D*, given by

$$D = d\bar{\varepsilon}_i / dm_i. \quad (1)$$

In Eq. (1) $m_i = \rho \cdot v_i$ where ρ is the liquid water density which equals to 1 g/cm^3, and v_i is the i-th segment volume. $d\bar{\varepsilon}_i$ defines the mean energy imparted by ionizing radiation to a segment. In addition to the absolute values of absorbed dose and energy imparted, we also introduce the mean values of these quantities. In this regard, the mean absorbed dose, $\overline{D}$, and mean energy imparted, $\bar{\varepsilon}$, are defined, respectively, as

$$\overline{D} = D/N_0 \quad \text{and} \quad \bar{\varepsilon} = \varepsilon/N_0. \quad (2)$$

Here, N_0 is the total number of particles traversing the water box.

The energy imparted can be used to determine the specific energy, z, which is the quotient of ε by *m*, assuming *m* as the mass of matter to which the energy is delivered. In our analysis, the specific energy is calculated for the total volume of the selected pyramidal neuron possessing the mass *M* as

$$z = \varepsilon/M, \quad (3)$$

where $M = \rho \cdot V$ and *V* is the total neuron volume.

In addition to the specific energy itself, the spectrum of specific energy is estimated as well. It is described as the frequency-mean specific energy, $\overline{z}_F$, and dose-mean specific energy, $\overline{z}_D$, which are obtained by the following formulas:

$$\overline{z}_F = \int z f(z) dz \quad \text{and} \quad \overline{z}_D = \int z^2 f(z) dz \Big/ \overline{z}_F. \quad (4)$$

In Eq. (4) *f*(z) is the frequency function of the specific energy.

In order to verify the microdosimetric calculations, the estimation of the lineal energy, y, is performed and the results are compared with works by other authors. According to (ICRU, 2011), y is the quotient of ε_S by $\bar{l}$, where ε_S is the energy imparted to the matter in a given volume by a single energy-deposition event and $\bar{l}$ is the mean chord length of that volume, therefore

$$y = \varepsilon_S / \bar{l}. \quad (5)$$

The frequency-mean lineal energy is the expected value of the lineal energies per single event taking into account all the secondary electrons produced by the primary events and all their interactions in the medium. It is given by

$$\bar{y}_F = \int y f(y) dy, \quad (6)$$

where $f(y)$ is the lineal energy distribution function.

2.3. Ion beam parameters

The unique patterns of energy depositions that occur within the CA1 pyramidal neuron are simulated by merging neuron spatial model and Monte Carlo models of HZE particle tracks. For this purpose, the tracks of ^{12}C and ^{56}Fe ions are simulated by using the beam parameters of several real experiments. In the present work, beam entrance parameters listed in Table 2 are taken from or calculated on the basis of experimental data produced at the Nuclotron of Joint Institute for Nuclear Research (Dubna, Russia) (Matveeva et al., 2013), Heavy Ion Medical Accelerator (HIMAC) of National Institute of Radiological Science (Chiba, Japan) (Imaoka et al., 2007; Wang et al., 2007), and Alternating Gradient Synchrotron (AGS) of Brookhaven National Laboratory (Long Island, New York, USA) (Huang, Smith, Cummings, Kendall, & Obenaus, 2009; Rabin, Joseph, & Shukitt-Hale, 2003; Sanchez, Nelson, & Green, 2010; Shukitt-Hale, Casadesus, Cantuti-Castelvetri, Rabin, & Joseph, 2003).

The particle tracks produced by the Geant4 Toolkit are oriented parallel with Z axis, as it is shown in Fig. 1. The total number of particles traversing the water box, N_0, is calculated using the fluence values from the mentioned experimental data. The distribution of the particle tracks within the XY plane of the box is set randomly. The area of the XY projection is estimated to be 2.34×10^{-3} cm^2. The targeting probability of radiations, P_{targ}, is calculated as the quotient of N_{targ} by N_0, where N_{targ} is the number of particles traversing the neuron.

2.4. Physics processes

In the present study, physics processes are represented as a natural extension of an electromagnetic model for radiobiology studies described elsewhere (Villagrasa, Francis, & Incerti, 2011). The tracks of primary ^{12}C and ^{56}Fe ions are simulated taking into account ionization processes. The secondary electrons with energies between 20 eV (i.e., extendable down to 0.025 eV) and 1 MeV are produced considering the ionization, elastic scattering, excitation (electronic and vibrational ones), and dissociative electron attachment. If the energy of electrons is greater than 1 MeV, we use the multiple scattering and ionization process from the "*Geant4 Standard EM Physics*" sub-library. These physical processes simulate direct radiation effects in the CA1 pyramidal neuron within 10^{-18}–10^{-15} s. The indirect effects occurring through the free radical formation are not considered in this study.

3. Results

3.1. Energy and absorbed dose distribution inside a targeted neuron

Figs. 2 and 3 show the spatial distributions of mean energy imparted and absorbed dose, respectively, inside the single CA1 pyramidal neuron traversed by ^{12}C and ^{56}Fe particles with different physical parameters. The plots depict five XY projections of energy and dose deposition patterns that correspond to irradiation with ion beams mentioned in Table 2. The accumulation of energy and radiation dose is appeared only inside the neuron. The distribution outside the cell is skipped. Higher values of the energy imparted and absorbed dose are depicted by "hotter" color-map areas that correspond to collisions resulting from the direct ^{12}C and ^{56}Fe particle traversals. The neuron segments receiving lower energy and dose are represented by "colder" areas arising predominantly as a consequence of secondary electron (i.e., delta ray) interactions.

As may be seen from Figs. 2 and 3, the irradiation by ^{56}Fe ions leads to the large number of events with very high values of the energy imparted and absorbed dose. The areas of maximum energy and dose deposition correspond to the orange and red zones in Figs. 2d, e, 3d, and e. Zones like these are practically absent in the case of ^{12}C ions (Figs. 2a–c and 3a–c) due to lower particles' LET.

3.2. Verification of microdosimetric calculations

Before estimation of stochastic quantities and their distributions, our microdosimetry calculations were verified against

Table 2 – Parameters of the ion beams used in microdosimetric calculations.

Particle	Energy, MeV/u	Dose, Gy	Fluence, $\times 10^6$ particles/cm^2	LET, keV/μm	N_0	N_{targ}	P_{targ},%	Accelerator facility
^{12}C	500	1.0	61.2	10.6	137067	11538	8.42	Nuclotron
^{12}C	290	0.2	9.8	13.0	21900	2058	9.40	HIMAC
^{12}C	290	2.0	96.3	13.0	215800	20820	9.65	HIMAC
^{56}Fe	1000	1.0	4.2	150.0	9400	3395	36.12	AGS
^{56}Fe	600	0.5	1.8	175.2	4020	1587	39.48	AGS

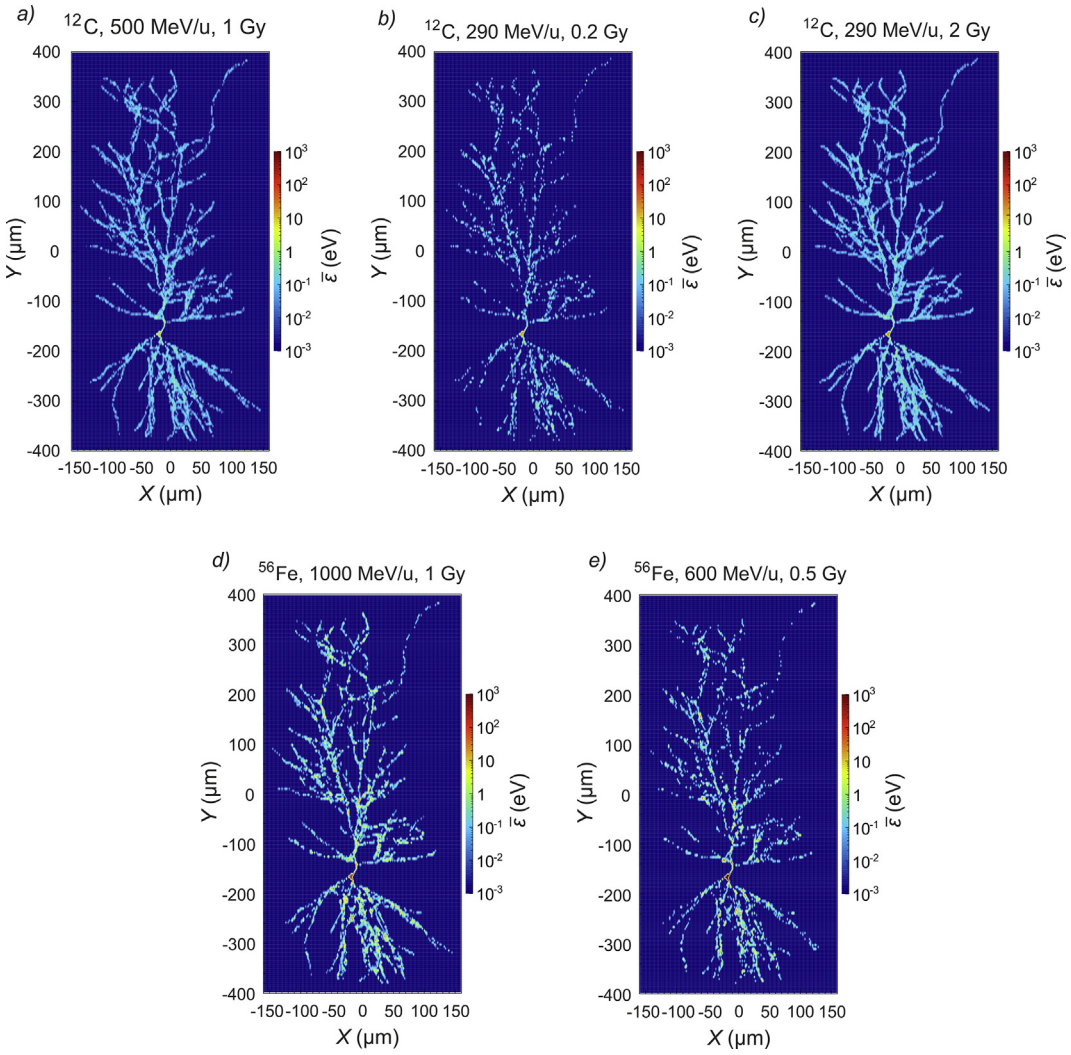

Fig. 2 – Spatial distribution of the mean energy imparted within the CA1 pyramidal neuron of the rat hippocampus (XY projection). Ion beam trajectories are directed along the Z-axis (perpendicular to the XY plane). The mean energy imparted, $\bar{\varepsilon}$, is indicated as a color-map and expressed in eV. The calculations are performed for irradiation with a) 1 Gy of 500 MeV/u ^{12}C ions; b) 0.2 Gy of 290 MeV/u ^{12}C ions; c) 2 Gy of 290 MeV/u ^{12}C ions; d) 1 Gy of 1000 MeV/u ^{56}Fe ions; e) 0.5 Gy of 600 MeV/u ^{56}Fe ions. The accumulation of the energy imparted is shown only inside the neuron. The energy distribution outside the cell is skipped.

the data on lineal energy spectra produced by Francis et al. (2012). Fig. 4 shows the results of our simulations for carbon ions of different LET in 1 μm diameter sphere filled with liquid water. The curves produced in the present work are consistent with those obtained by Francis et al. (2012). It gives a reason to believe that the basic principles of our microdosimetric calculations are correct.

3.3. *Distributions of stochastic quantities*

Fig. 5 provides the graphs of energy imparted distributions observed within a single pyramidal neuron under exposure to the mentioned ion beams. This data can be presented as the frequency function $f(\varepsilon)$ versus the energy imparted itself. Zero values of $f(\varepsilon)$ are excluded from the analysis. In these plots, discrete data sets are approximated by polynomial functions $f(\varepsilon) = a_0 + a_1\varepsilon + a_2\varepsilon^2 + a_3\varepsilon^3 + a_4\varepsilon^4 + a_5\varepsilon^5 + a_6\varepsilon^6$ with the parameters stated in Table 3. These functions are the downward and double-shaped curves that have maxima (peak) and minima (trough). The positions of peaks and troughs depend on physical parameters of ion beams. In the case of ^{12}C, minima of the continuous functions are observed at 79 keV for 0.2 and 2.0 Gy of 290 MeV/u ions and 59 keV for 1 Gy of 500 MeV/u ions. Maxima are detected at 134 keV (0.2 Gy, 290 MeV/u), 138 keV (2.0 Gy, 290 MeV/u), and 101 keV (1 Gy, 500 MeV/u). Comparison between data for 0.2 and 2 Gy of 290 MeV/u carbon ions shows a difference in the energy deposition patterns resulting from 10-times increase in radiation dose (Fig. 5a). The significant change is revealed only in the curve amplitude. The shift of curves in relation to the energy imparted is not observed. As for the ^{56}Fe particles, positions of troughs are calculated to be at 883 and 786 keV for 600 and 1000 MeV/u ions, respectively. Peaks are observed at 1705 keV (600 MeV/u) and 1375 keV (1000 MeV/u).

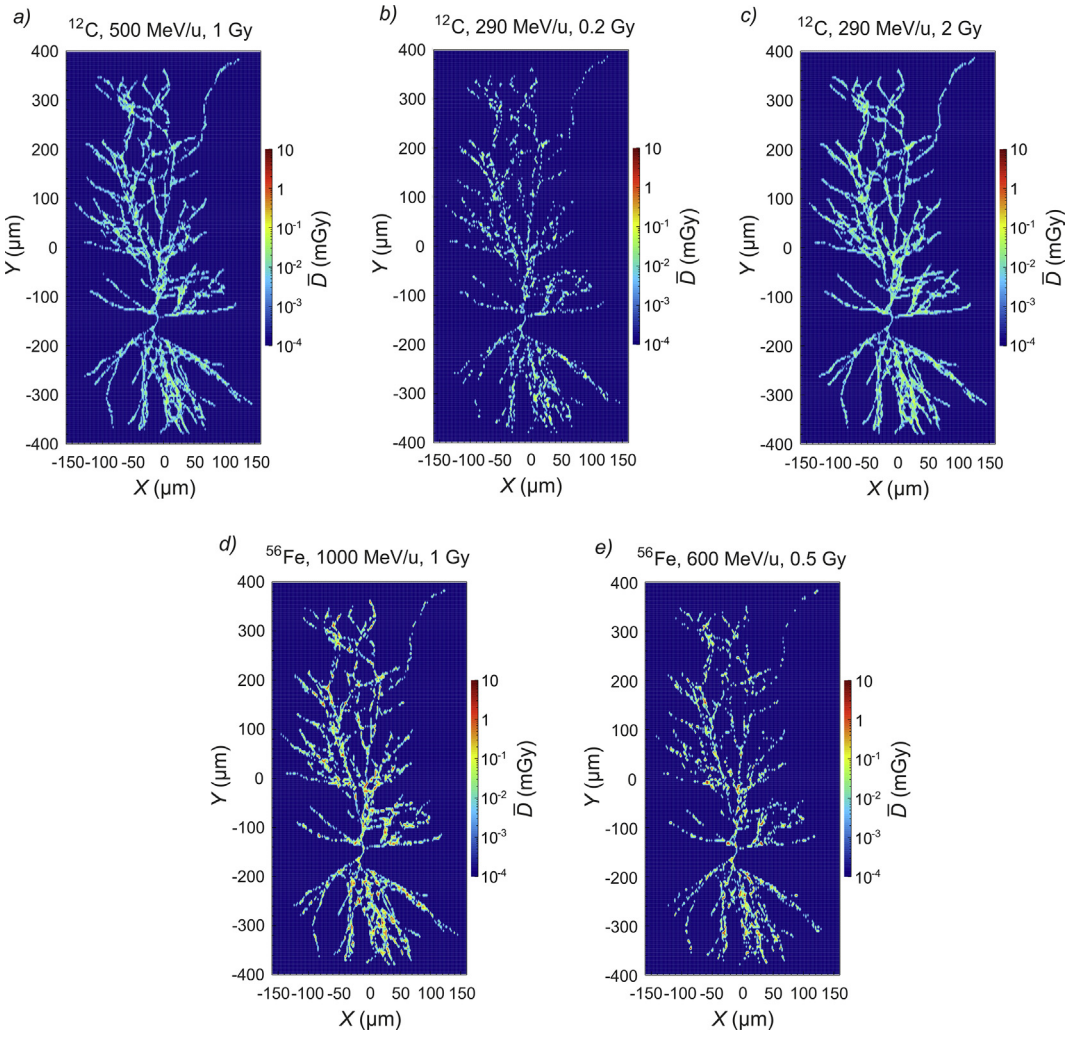

Fig. 3 – Spatial distribution of the absorbed dose within the CA1 pyramidal neuron of the rat hippocampus (XY projection). The ion beam trajectories are directed along the Z-axis (perpendicular to the XY plane). The mean absorbed dose, $\bar{D}$, is indicated as a color-map and expressed in mGy. Calculations are performed for irradiation with a) 1 Gy of 500 MeV/u ^{12}C ions; b) 0.2 Gy of 290 MeV/u ^{12}C ions; c) 2 Gy of 290 MeV/u ^{12}C ions; d) 1 Gy of 1000 MeV/u ^{56}Fe ions; e) 0.5 Gy of 600 MeV/u ^{56}Fe ions. The accumulation of radiation dose is shown only inside the neuron. The dose distribution outside the cell is skipped.

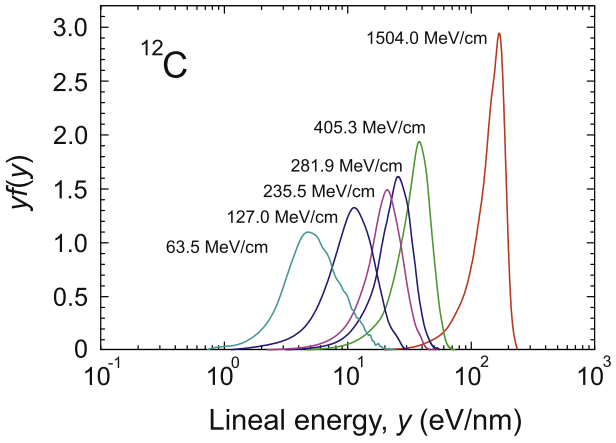

Fig. 4 – Lineal energy spectra of ^{12}C ions calculated in 1 μm diameter sphere and for different LET values which are displayed on the plot.

In our calculations, specific energy spectra of the selected ions are represented as discrete values of the function z f(z) (Fig. 6). In the case of ^{12}C particles, the maxima of z f(z) are observed at 0.05 mGy (500 MeV/u, 1 Gy), 0.06 mGy (290 MeV/u, 2 Gy), and 0.08 mGy (290 MeV/u, 0.2 Gy). Irradiation with ^{56}Fe ions results in the shift of maxima towards the higher values of specific energy equaling to 1.1 mGy (1000 MeV/u, 1 Gy) and 1.3 mGy (600 MeV/u, 0.5 Gy).

4. Discussion

In the present work the Monte-Carlo simulation technique is used to estimate unique energy deposition patterns in a single neural cell under exposure to HZE particles. For the analysis, ion beams with characteristics comparable to GSR spectra are selected. More precisely, the parameters of the particles are chosen as in realistic ground-based experiments with animals

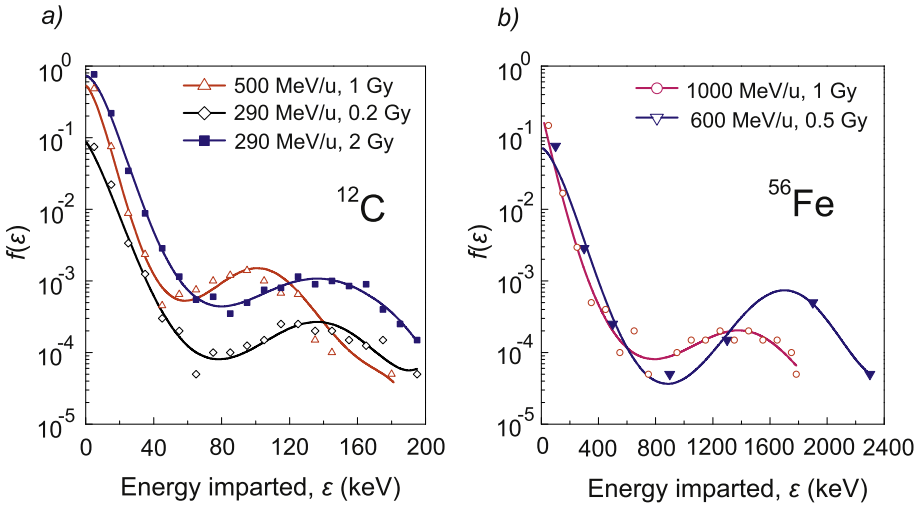

Fig. 5 – Distributions of non-zero energy imparted values in the single CA1 pyramidal neuron under exposure to ^{12}C (a) and ^{56}Fe (b) ion beams. The discrete data sets are approximated by the polynomial functions $f(\varepsilon) = a_0 + a_1\varepsilon + a_2\varepsilon^2 + a_3\varepsilon^3 + a_4\varepsilon^4 + a_5\varepsilon^5 + a_6\varepsilon^6$ with the parameters presented in Table 3.

Table 3 – Parameters of the function $f(\varepsilon) = a_0 + a_1\varepsilon + a_2\varepsilon^2 + a_3\varepsilon^3 + a_4\varepsilon^4 + a_5\varepsilon^5 + a_6\varepsilon^6$ approximating the calculated energy imparted distributions.

Parameter	Value				
	^{12}C, 290 MeV/u, 0.2 Gy	^{12}C, 290 MeV/u, 2 Gy	^{12}C, 500 MeV/u, 1 Gy	^{56}Fe, 1000 MeV/u, 1 Gy	^{56}Fe, 600 MeV/u, 0.5 Gy
a_0	−1.04487	−0.12778	−0.26236	−0.63883	−1.05872
a_1	−1.04487	−0.00775	−0.02338	−0.00831	−0.00184
a_2	−0.00124	−0.00286	−0.00393	1.13135×10^{-6}	-1.54091×10^{-5}
a_3	2.63634×10^{-5}	5.85926×10^{-5}	1.08149×10^{-4}	1.00013×10^{-8}	2.39278×10^{-8}
a_4	-1.65337×10^{-7}	-4.71263×10^{-7}	-1.10194×10^{-6}	-7.81692×10^{-12}	-1.19133×10^{-11}
a_5	3.35509×10^{-10}	1.72753×10^{-9}	4.9239×10^{-9}	1.6648×10^{-15}	1.93842×10^{-15}
a_6	0.0	-2.42722×10^{-12}	-8.14525×10^{-12}	0.0	0.0

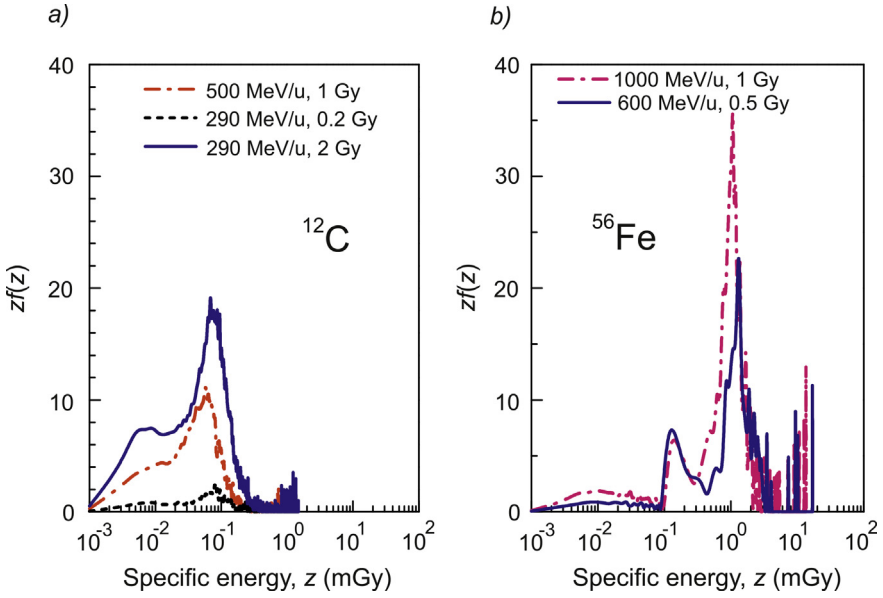

Fig. 6 – Specific energy spectra in the single CA1 pyramidal neuron under exposure to ^{12}C (a) and ^{56}Fe (b) ions.

aimed to study radiation-induced damage to CNS. In this regard, our calculations may help in establishing a link between radiation damage at the level of a single neuron and certain cognitive impairments.

The selection of the hippocampal neurons are motivated by increasing the body of experimental findings supporting the key role of the brain structure in radiation-induced cognitive impairments. In rodents the hippocampus is responsible mainly for the short and long-term memory, spatial memory and navigation. These CNS functions are observed to change after exposure to HZE nuclei (Cucinotta et al., 2014). Pyramidal neurons of the CA1 hippocampal region have a complicated spatial composition. The dendritic tree accumulates the largest portion of energy compared to the soma. Therefore, the patterns of energy and dose deposition within these neurons are completely different from those in other cells that do not possess such a complicated structure.

Hippocampus-dependent cognitive impairments are observed at relatively low doses of HZE particles (0.4–2 Gy) that do not lead to any significant perturbance of neurogenesis (Rola et al., 2004, 2005, 2008). These findings suggest that observed CNS malfunctions can be a result of changes in neurotransmission and synaptic plasticity (Machida, 2009; Machida, Lonart, & Britten, 2010). Indeed, some experiments with rodents revealed that heavy charged particles may alter the long-term potentiation at CA1 synapses of the hippocampus (Vlkolinsky et al., 2007). In this regard, the patterns of energy and dose deposition obtained in our study may also suggest a possibility of radiation damage to synapses. Large energy deposition in small volumes most likely enables HZE nuclei to induce violations in the synaptic active zone. Although the precise mechanism of radiation effects on synapses is unknown, it can be hypothesized that synaptic transmission may be disturbed via overproduction of free radical species as well as direct interaction of charged particles with certain sensitive structures in the synaptic zone. Further development of our simulation technique will permit to estimate the yields of radiolytic species in a single neuron and, in particular, in synapses.

In the present paper, we evaluated two microdosimetric quantities that describe the results of the processes by which particle energy is converted and finally deposited in matter. For the analyses, we selected the energy imparted and specific energy. Since the calculations are performed for relatively thin structures, like dendritic tree segments, these quantities are estimated in terms of their distribution. In the case of such small targets, stochastic variations of a quantity would be important for comprehensive understanding of energy deposition patterns within a single neuron.

According to our calculations, the distribution of the energy imparted depends on number of particles traversing the neuron as well as on type of ions and their kinetic energy. The former of these two factors is determined mainly by the fluence of particles, radiation dose and cell morphology. Meanwhile, the microdosimetric distribution of the energy imparted to the cell determines the particles' RBE (Tunga, Liu, Wang, & Chang, 2004). For that reason, the computation of this stochastic quantity for neural cells may be essential for revealing the effect of the neuron's complicate spatial structure on the RBE value.

The abovementioned factors influence as well the specific energy spectra. The knowledge of the specific energy distribution corresponding to a certain absorbed dose can be important, as in the irradiated mass element the effects of the radiation can be more closely related to z than to D. The values of z may differ greatly from D for small mass values, for example, when certain components of a neural cell are considered (ICRU, 2011).

Our microdosimetric calculations are verified against the data by other authors who evaluated the lineal energy spectra for HZE particles in a small sphere filled with liquid water. The similarity of the computed curves to the results by Francis et al. (2012) proves the correctness of our simulation.

The results provided are of particular importance for the problems of hadron beam therapy. In case of brain tumors, the study of radiation damage to single neurons would be helpful for revealing the factors determining the side effects of the treatment. The estimation of dose deposition to neural cells surrounding the treated area may be essential for the prediction of further processes of neuron death and the development of cognitive impairments. Finally, since CNS is one of the most critical systems associated with the radiation damage by HZE particles, the methods reviewed in this paper may contribute to the ongoing studies on space radiation risk assessment.

Acknowledgments

The work was partially supported by the Grants #14-091-01 and #14-092-04 of Joint Institute for Nuclear Research, the JINR-ARE Project # 301 "Mathematical Modelling of Genetic Regulatory Networks in Bacterial and Higher Eukaryotic Cells". The authors also acknowledge the scientific support within the project # 4333-9-13/14 between Joint Institute for Nuclear Research and National University of Mongolia.

REFERENCES

Agostinelli, S., Allison, J., Amako, K., Apostolakis, J., Araujo, H., Arce, P., et al. (2003). Geant4 – a simulation toolkit. *Nuclear Instruments and Methods A, 506*, 250–303. http://dx.doi.org/10.1016/S0168-9002(03)01368-8.

Allison, J., Amako, K., Apostolakis, J., Araujo, H., Dubois, P. A., Asai, M., et al. (2006). Geant4 developments and applications. *IEEE Transactions on Nuclear Science, 53*(1), 270–278. http://dx.doi.org/10.1109/TNS.2006.869826.

Ascoli, G. A. (2006). Mobilizing the base of neuroscience data: the case of neuronal morphologies. *Nature Reviews Neuroscience, 7*, 318–324.

Bannerman, D. M., Sprengel, R., Sanderson, D. J., McHugh, S. B., Rawlins, J. N., Monyer, H., et al. (2014). Hippocampal synaptic plasticity, spatial memory and anxiety. *Nature Reviews Neuroscience, 15*, 181–192. http://dx.doi.org/10.1038/nrn3677.

Britten, R. A., Davis, L. K., Johnson, A. M., Keeney, S., Siegel, A., Sanford, L. D., et al. (2012). Low (20 cGy) doses of 1 GeV/u ^{56}Fe-particle radiation lead to a persistent reduction in the spatial learning ability of rats. *Radiation Research, 177*, 146–151.

Carnevale, N. T., Tsai, K. Y., Claiborne, B. J., & Brown, T. H. (1997). Comparative electrotonic analysis of three classes of rat

hippocampal neurons. *Journal of Neurophysiology, 78*(2), 703–720.
Cucinotta, F. A., Alp, M., Sulzman, F. M., & Wang, M. (2014). Space radiation risks to the central nervous system. *Life Sciences in Space Research, 2*, 54–69.
Cucinotta, F. A., Nikjoo, H., & Goodhead, D. T. (1998). Comment on the effects of delta-rays on the number of particle-track transversals per cell in laboratory and space exposures. *Radiation Research, 150*, 115–119.
Cucinotta, F. A., Townsend, L. W., Wilson, J. W., Golightly, M. J., & Weyland, M. (1994). Analysis of radiation risk from alpha particle component of solar particle events. *Advances in Space Research, 10*, 661–670.
Cucinotta, F. A., Wang, H., & Huff, J. L. (2009). Risk of acute or late central nervous system effects from radiation exposure. In J. C. McPhee, & J. B. Charles (Eds.), *Human health and performance risks of space exploration missions* (pp. 191–212). Houston: Lyndon B. Johnson Space Center.
Curtis, S. B., Vazquez, M. E., Wilson, J. W., Atwell, W., Kim, M., & Capala, J. (1998). Cosmic ray hit frequencies in critical sites in the central nervous system. *Advances in Space Research, 22*(2), 197–207.
Francis, Z., Incerti, S., Ivanchenko, V., Champion, C., Karamitros, M., Bernal, M. A., et al. (2012). Monte Carlo simulation of energy-deposit clustering for ions of the same LET in liquid water. *Physics in Medicine & Biology, 57*(1), 209–224. http://dx.doi.org/10.1088/0031-9155/57/1/209.
Gauger, G. E., Tobias, C. A., Yang, T., & Whitney, M. (1986). The effect of space radiation on the nervous system. *Advances in Space Research, 6*(11), 243–249.
Huang, L., Smith, A., Cummings, P., Kendall, E. J., & Obenaus, A. (2009). Neuroimaging assessment of memory-related brain structures in a rat model of acute space-like radiation. *Journal of Magnetic Resonance Imaging, 29*, 785–792.
ICRU. (2011). Report 85: fundamental quantities and units for ionizing radiation. *Journal of the ICRU, 11*(1), 1–31.
Imaoka, T., Nishimura, M., Kakinuma, S., Hatano, Y., Ohmachi, Y., Yoshinaga, S., et al. (2007). High relative biologic effectiveness of carbon ion radiation on induction of rat mammary carcinoma and its lack of H-ras and Tp53 mutations. *International Journal of Radiation Oncology, Biology, Physics, 69*(1), 194–203.
Kim, M. H., Wilson, J. W., Simonsen, L. C., Cucinotta, F. A., Atwell, W., Badavi, F. F., et al. (1999). *Contribution of high charge and energy (HZE) ions during solar-particle event of September 19, 1989*. NASA TP-1999-209320. Houston: NASA Johnson Space Center
Latocha, M., Autischer, M., Beck, P., Bottolier–Depois, J. F., Rollet, S., & Trompier, F. (2007). The results of cosmic radiation in-flight TEPC measurements during the CAATER flight campaign and comparison with simulation. *Radiation Protection Dosimetry, 125*(1–4), 412–415.
Machida, M. (2009). *Effects of HZE irradiation on chemical neurotransmission in rodent hippocampus* (PhD thesis). Eastern Virginia Medical School. East Eisenhower Parkway: ProQuest LLC.
Machida, M., Lonart, G., & Britten, R. (2010). Low (60 cGy) doses of 56Fe HZE-particle radiation lead to a persistent reduction in the glutamatergic readily releasable pool in rat hippocampal synaptosomes. *Radiation Research, 174*, 618–623. http://dx.doi.org/10.1667/RR1988.1.
Matveeva, M. I., Shtemberg, A. S., Timoshenko, G. N., Krasavin, E. A., Narkevich, V. B., Klodt, P. M., et al. (2013). The effects of irradiation by ^{12}C carbon ions on monoamine exchange in several rat brain structures. *Neurochemical Journal, 7*(4), 303–307. http://dx.doi.org/10.1134/S1819712413040065.
NCRP. (1989). *Guidance on radiation received in space activities*. NCRP report no. 98. Bethesda, MD: NCRP.
Okamoto, H., Kanai, T., Kase, Y., Matsumoto, Y., Furusawa, Y., Fujita, Y., et al. (2011). Relation between lineal energy distribution and relative biological effectiveness for photon beams according to the microdosimetric kinetic model. *Journal of Radiation Research, 52*(1), 75–81. http://dx.doi.org/10.1269/jrr.10073.
Palajová, Z., Spurny, F., & Davídková, M. (2006). The comparison of calculated and experimental microdosimetric distributions for carbon ions. *Radiation Protection Dosimetry, 122*(1–4), 491–493.
Rabin, B. M., Joseph, J. A., & Shukitt-Hale, B. (2003). Long-term changes in amphetamine-induced reinforcement and aversion in rats following exposure to ^{56}Fe particle. *Advances in Space Research, 31*, 127–133.
Rola, R., Fishman, K., Baure, J., Rosi, S., Lamborn, K. R., Obenaus, A., et al. (2008). Hippocampal neurogenesis and neuroinflammation after cranial irradiation with ^{56}Fe particles. *Radiation Research, 169*(6), 626–632.
Rola, R., Otsuka, S., Obenaus, A., Nelson, G. A., Limoli, C. L., VandenBerg, S. R., et al. (2004). Indicators of hippocampal neurogenesis are altered by ^{56}Fe-particle irradiation in a dose-dependent manner. *Radiation Research, 162*, 442–446.
Rola, R., Sarkissian, V., Obenaus, A., Nelson, G. A., Otsuka, S., Limoli, C. L., et al. (2005). High-LET irradiation induces inflammation and persistent changes in markers of hippocampal neurogenesis. *Radiation Research, 164*, 556–560.
Rollet, S., Colautti, P., Grosswendt, B., Herault, J., Wind, M., Gargioni, E., et al. (2011). Microdosimetric assessment of the radiation quality of a therapeutic proton beam: comparison between numerical simulation and experimental measurements. *Radiation Protection Dosimetry, 143*, 445–449.
Rudobeck, E., Nelson, G. A., Sokolova, I. V., & Vlkolinský, R. (2014). $^{28}Silicon$ radiation impairs neuronal output in CA1 neurons of mouse ventral hippocampus without altering dendritic excitability. *Radiation Research, 181*, 407–415.
Sanchez, M. C., Nelson, G. A., & Green, L. M. (2010). Effects of protons and HZE particles on glutamate transport in astrocytes, neurons and mixed cultures. *Radiation Research, 174*(6a), 669–678.
Schardt, D., Elsasser, T., & Schulz-Ertner, D. (2010). Heavy-ion tumor therapy: physical and radiobiological benefits. *Reviews of Modern Physics, 82*, 383–417.
Schmid, E., & Schrader, T. (2007). Different biological effectiveness of ionising and non-ionising radiations in mammalian cells. *Advances in Space Research, 5*, 1–4.
Shukitt-Hale, B., Casadesus, G., Cantuti-Castelvetri, I., Rabin, B. M., & Joseph, J. A. (2003). Cognitive deficits induced by ^{56}Fe radiation exposure. *Advances in Space Research, 31*(1), 119–126.
Townsend, L. W., Cucinotta, F. A., Wilson, J. W., & Bagga, R. (1994). Estimates of HZE particle contributions to SPE radiation exposures on interplanetary missions. *Advances in Space Research, 10*, 671–674.
Tunga, C. J., Liu, C. S., Wang, J. P., & Chang, S. L. (2004). Calculations of cellular microdosimetry parameters for alpha particles and electrons. *Applied Radiation and Isotopes, 61*, 739–743.
Villagrasa, C., Francis, Z., & Incerti, S. (2011). Physical models implemented in the GEANT4-DNA extension of the GEANT-4 toolkit for calculating initial radiation damage at the molecular level. *Radiation Protection Dosimetry, 143*, 214–218.
Vlkolinsky, R., Krucker, T., Smith, A. L., Lamp, T. C., Nelson, G. A., & Obenaus, A. (2007). Effects of lipopolysaccharide on ^{56}Fe-particle radiation-induced impairment of synaptic plasticity in the mouse hippocampus. *Radiation Research, 168*, 462–470.
Wang, B., Murakami, M., Eguchi-Kasai, K., Nojima, K., Shang, Y., Tanaka, K., et al. (2005). Effects of prenatal irradiation with an accelerated heavy-ion beam on postnatal development in rats:

I. Neurophysiological alterations. *Radiation Research, 164*(4 Pt 2), 561–566.

Wang, B., Murakami, M., Eguchi-Kasai, K., Nojima, K., Shang, Y., Tanaka, K., et al. (2007). Effects of prenatal irradiation with accelerated heavy-ion beams on postnatal development in rats: III. Testicular development and breeding activity. *Advances in Space Research, 40*, 550–562.

Wiebel, B. (1994). *Chemical composition in high energy cosmic rays*. University of Wuppertal report WUB 94-08. Wuppertal: University of Wuppertal.

Yasuda, H., Komiyama, T., & Fujitaka, K. (2001). Probability of hippocampus cell hits by high-LET space radiation in a low-Earth-orbit mission (STS-91). *Physica Medica, 17*(Suppl.), 166–169.

Yasuda, T., Oda, S., Yasuda, H., Hibi, Y., Anzai, K., & Mitani, H. (2011). Neurocytotoxic effects of iron-ions on the developing brain measured in vivo using medaka (*Oryzias latipes*), a vertebrate model. *International Journal of Radiation Biology, 87*(9), 915–922.